



# An assessment of juvenile sand tiger (*Carcharias taurus*) activity patterns in a seasonal nursery using accelerometer transmitters

Jeff Kneebone · Megan Winton · Andy Danylchuk ·  
John Chisholm · Gregory B. Skomal

Received: 6 November 2017 / Accepted: 3 October 2018  
© Springer Nature B.V. 2018

**Abstract** Telemetry transmitters incorporating accelerometers have recently emerged as powerful tools for investigating the activity patterns of individuals and groups of individuals in nearshore environments. Data obtained from these devices provide not only a time series of animal occurrence at acoustic receivers, but also a direct measure of animal activity, which can be used to quantify trends in activity states over time and in relation to exogenous factors. Here we used passive acoustic accelerometry to examine trends in the activity and swimming depth of eight juvenile sand tigers (*Carcharias taurus*) in Plymouth, Kingston, Duxbury (PKD) Bay, Massachusetts, USA, a recently identified nursery area. We applied a novel geostatistical modeling approach that accounts for both latent spatial and individual variation to assess the effects of time of day, tidal

stage, water temperature, and lunar phase on activity patterns at both a population- and individual-level. The best-fitting model indicated that juvenile sand tigers were more active and more likely to be detected at the surface at night and during the new moon; water temperature was also a predictor of surface activity. Collectively, our results confirm conventional wisdom that sand tigers are slow-moving fish that are more active at night and provide evidence that high activity in PKD Bay may be indicative of foraging activity.

**Keywords** Acoustic telemetry · Accelerometer · Geostatistical mixed effects model · Spatial variation · Individual variability · Spatial random effects

## Introduction

Estuarine systems and shallow bays are dynamic areas that provide critical habitat for many coastal shark species (Knip et al. 2010). Studies investigating the spatial ecology of individuals or groups of individuals in these nearshore habitats often rely on location data collected using passive acoustic telemetry (see Heupel et al. 2006 for a description of this technique) to describe horizontal movements and space use in relation to environmental factors (e.g., Ubeda et al. 2009; Simpfendorfer et al. 2011; reviewed by Schlaff et al. 2014). Behaviors and activity patterns can sometimes be inferred based on metrics derived from location estimates (Pedersen et al. 2011; McKellar et al. 2015). However, studies employing position-only telemetry transmitters often

J. Kneebone (✉)  
Anderson Cabot Center for Ocean Life, New England Aquarium,  
Central Wharf, Boston, MA 02110, USA  
e-mail: jeff.kneebone@gmail.com

M. Winton  
Department of Fisheries Oceanography, School for Marine  
Science and Technology, University of Massachusetts Dartmouth,  
836 South Rodney French Blvd, New Bedford, MA 02744, USA

A. Danylchuk  
Department of Environmental Conservation, University of  
Massachusetts Amherst, 160 Holdsworth Way, Room 311,  
Amherst, MA 01003, USA

J. Chisholm · G. B. Skomal  
Massachusetts Marine Fisheries, 836 South Rodney French Blvd,  
New Bedford, MA 02744, USA

lack the context needed to quantify the behavioral and physiological interactions underlying observed space use, which is critical for understanding, interpreting, and evaluating how species respond to changing environmental conditions (Whitney et al. 2012).

Acoustic telemetry transmitters incorporating tri-axial accelerometers have become an increasingly popular tool for examining the activity patterns of coastal marine species (O'Toole et al. 2010; Murchie et al. 2011; Barnett et al. 2016). Detection data obtained from these devices not only provide a time series of animal occurrence at acoustic receivers, but also a direct measure of animal activity (via changes in acceleration), which can be used to quantify trends in activity states over time (Taylor et al. 2013; Stehfest et al. 2015; Kolarevic et al. 2016), associations with environmental conditions (Wilson et al. 2014; Papastamatiou et al. 2015; Payne et al. 2016), and to infer energy expenditure (Wilson et al. 2013; Brodie et al. 2016; Brownscombe et al. 2017). Unlike archival accelerometers, which record high resolution data on animal activity over relatively brief periods (e.g., hours to weeks; Gleiss et al. 2010; Whitney et al. 2010; Lear et al. 2016), acoustic accelerometer transmitters typically provide coarser-scale data (i.e., at transmission intervals of 1–2 min) and have battery lives that are better suited for monitoring activity patterns within areas of receiver coverage over longer time periods (e.g., weeks to months; Burnett et al. 2014). The ability to quantify long-term activity patterns is particularly important when monitoring tagged animals in dynamic nearshore areas, where individual activity may be influenced by short- (e.g., tidal, diel; Whitney et al. 2007) and long-term (e.g., seasonal; Kneebone et al. 2012) physical and environmental factors over a range of spatial scales. Given the anthropogenic threats facing these ecologically sensitive areas (McLusky and Elliott 2004), a more holistic understanding of animal activity in these environments is important for management and conservation efforts (Beck et al. 2001), particularly for areas that support threatened or endangered species (Brownscombe et al. 2015; Gleiss et al. 2017).

The sand tiger (*Carcharias taurus*) is a large coastal shark that ranges from the Gulf of Mexico to the Gulf of Maine in the western North Atlantic Ocean (WNA; Bigelow and Schroeder 1953). Within this broad area, sand tigers occur in nearshore and offshore habitats, with juveniles commonly inhabiting littoral areas such as shallow inshore bays, estuaries, and river mouths (Compagno 2001; Collette and Klein-MacPhee 2002;

Kneebone et al. 2012). In response to purported 80–90% population declines in the 1980's and 1990's (Musick et al. 1993; Castro et al. 1999; Musick et al. 2000), managers prohibited the harvest of the species in both U.S. federal (NMFS 1999) and state (ASMFC 2008) waters. While the current status of the population in the WNA remains uncertain (Carlson et al. 2009), the species is listed as a 'Species of Concern' due to its exceptionally low biological productivity (Gilmore et al. 1983) and sensitivity to anthropogenic disturbance in nearshore habitats (Carlson et al. 2009).

Recently, Plymouth, Kingston, Duxbury (PKD) Bay, Massachusetts, USA, a tidal estuary located in the western Gulf of Maine, was identified as a seasonal nursery area in which juvenile sand tigers remain resident for the summer months (June – October) and exhibit strong site fidelity to specific habitats on an intra- and inter-annual basis (Kneebone et al. 2012). Due to its ecological importance as a nursery area and susceptibility to anthropogenic disturbance, PKD Bay was designated as a juvenile sand tiger Habitat Area of Particular Concern (HAPC) by the National Oceanic and Atmospheric Administration (NMFS 2017). Despite this distinction, little is known about the fine-scale activity patterns of juvenile sand tigers within this embayment, or in similar habitats throughout the species' global range. Given the importance of shark nursery areas to population recovery and maintenance (Heithaus 2007; Heupel et al. 2007), declines in the WNA sand tiger population, and the designation of PKD Bay as a HAPC, a thorough assessment of the activity patterns of juvenile sand tigers in this sensitive coastal habitat is warranted. The objective of this study was to use passive acoustic accelerometry to assess the effects of physical and environmental factors on sand tiger activity patterns in PKD Bay.

## Materials and methods

### Study site

PKD Bay is a relatively productive coastal embayment located along the south shore of Massachusetts, USA (Fig. 1). The system is highly tidal, experiencing semi-diurnal tides with mean amplitudes of 3.2 m that result in a 66.1% tidal exchange in water volume and fluctuation in total surface area from 22.1 to 40.7 km<sup>2</sup> at mean low and mean high water, respectively (Iwanowicz et al. 1974). Bottom substrates in PKD Bay consist of shallow

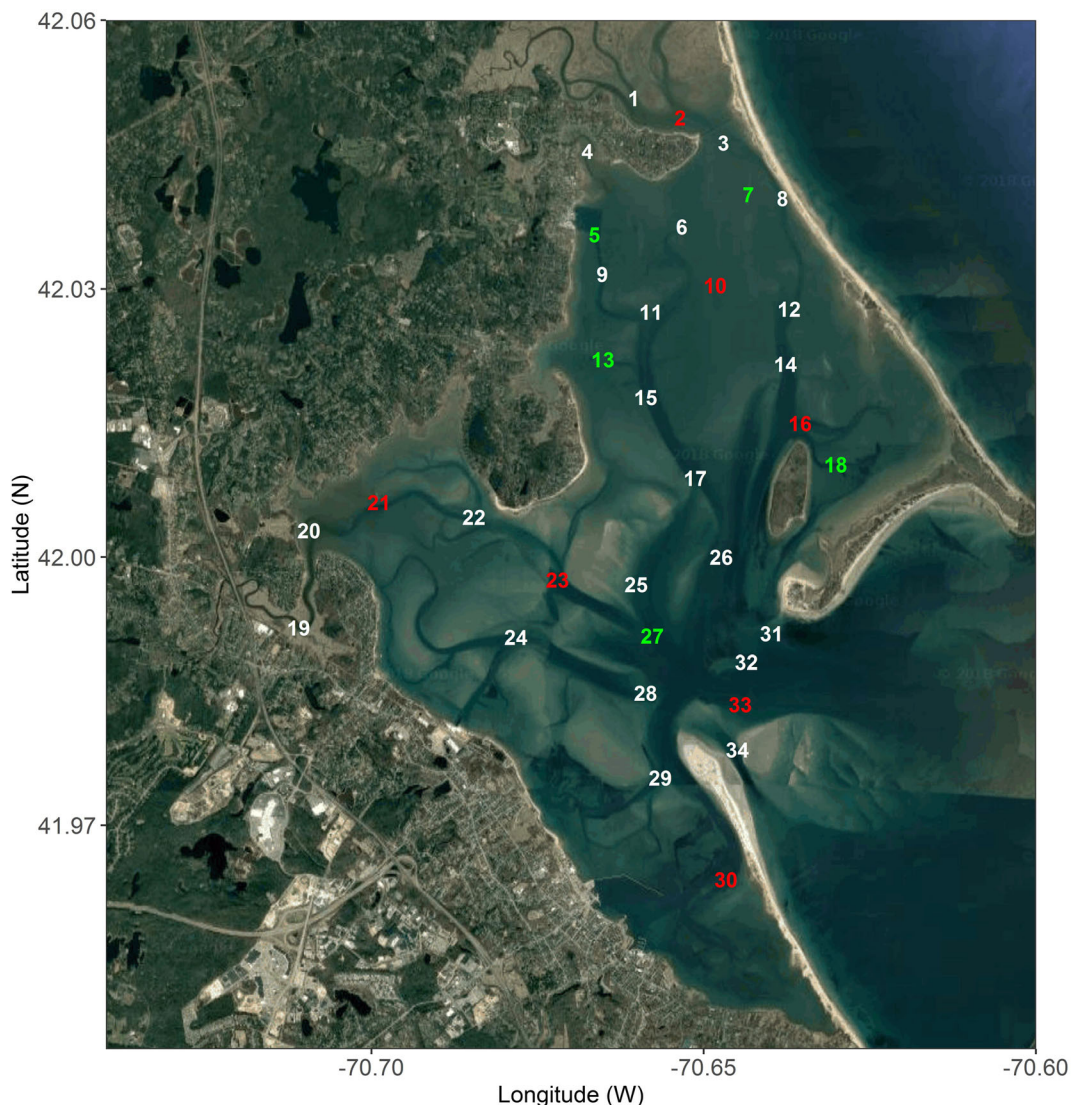


**Fig. 1** Receiver deployment locations in Plymouth, Kingston, Duxbury Bay. Receivers with temperature (red) and temperature

and light sensor loggers (green) are indicated. Map made using the “ggmap” library (Kahle and Wickham 2013) in R

eelgrass beds, sand flats that are exposed at low tide, and deep (5–10 m) channels. Average overall depth ranges from 2.1 to 3.3 m between mean low and mean high water, respectively, with maximum depths of 20 m near the mouth of the bay.

#### Shark capture and tagging

Juvenile sand tigers were captured in PKD Bay from a small (6.1 m) center console research vessel in July 2011 using conventional rod and reel tackle, circle hooks (size

8/0), and chunks of menhaden (*Brevoortia tyrannus*) for bait. All sharks were captured, handled, and released in accordance with Massachusetts Division of Marine Fisheries regulations. Once each shark was landed, the hook was removed (if possible), and tonic immobility was induced by restraining the shark ventral side up (Watsky and Gruber 1990) in a V-shaped table lined with pre-wetted neoprene. Sharks were tagged with two models of individually-coded 69 kHz Vemco acoustic transmitters (model V9AP-2 L, nominal delay = 60–180 s, battery life = 123 days; model V9AP-2H,

nominal delay = 60–180 s, battery life = 81 days; Vemco Division, AMIRIX Systems Inc., Halifax, Nova Scotia) containing tri-axial accelerometers (Measurement Range:  $\pm 29.4 \text{ m s}^{-2}$ ; Vector Range: 0.000–3.463  $\text{m s}^{-2}$ ) and pressure (i.e. depth) sensors (Range: 0.00–50.00 m; Accuracy:  $\pm 1.70 \text{ m}$ ; Resolution: 0.08 m). Both transmitter models measured acceleration on three axes five times per second over a defined sampling interval (V9AP-2 L: 54 s sampling interval; V9AP-2H: 57 s sampling interval) and transmitted the value that represents the root mean square (RMS) acceleration resulting from the contribution of each of the three axes over that interval. The resulting RMS acceleration value is intended as a general activity index of the body of a fish, or overall dynamic body acceleration (ODBA).

Transmitters were implanted in the body cavity through a small (2–3 cm) abdominal incision on the ventral side of the shark along the midline, anterior to the pelvic fins. Care was taken to ensure that transmitters were oriented along the anterior-posterior axis of the fish to reduce error and improve the signal-to-noise ratio of the accelerometer output (Watanuki et al. 2003; Gleiss et al. 2011). Incisions were closed with 3 or 4 interrupted sutures (2–0 PDS II, Ethicon Inc., NJ). Prior to release, fork length (FL; cm) and sex were recorded for each individual. All surgical procedures were completed within 5–10 min. All capture and sampling methods conducted in this study were approved under the University of Massachusetts Dartmouth Institutional Animal Care and Use Committee Protocol Number 10–01.

#### Receiver deployment and acoustic monitoring

To assess movement and activity patterns of juvenile sand tigers within PKD Bay, a fixed array of 34 acoustic receivers (model VR2W, Vemco Division, AMIRIX Systems Inc., Halifax, Nova Scotia) was deployed from June to October 2011 (Fig. 1; see Kneebone et al. 2012 for details). On average, the detection radius of receivers ranged from ~100 m in water depths <3 m to ~350 m in water depths >5 m (based on range tests conducted by Kneebone et al. 2012). Receivers were downloaded and cleaned monthly during each deployment period.

To monitor water temperature within PKD Bay throughout the study period, 12 temperature loggers (model HOBO Pendant, Onset Computer Corporation, Onset, MA) were deployed on acoustic receiver moorings (Fig. 1). All loggers were set to record temperature

(°C) every 30 min (on the half hour and hour) with an accuracy of  $\pm 0.7 \text{ °C}$  (Range:  $-20 - 70 \text{ °C}$ ). Five of these temperature loggers also recorded light intensity (Range: 0–320,000 lx) at the same interval (Fig. 1).

#### Accelerometer calibration

To investigate the relationship between raw acceleration values and biologically-relevant activity states, calibration experiments were conducted using two juvenile sand tigers measuring 82 cm (female; ST1108) and 97 cm (male; ST1115). During collection, both sharks were hooked in the mouth and free of physical trauma. Following capture, sharks were held in aerated onboard coolers and transported to a 5700 L outdoor holding tank at the Jones River Landing Environmental Heritage Center in Kingston, MA; transport times for both sharks were under 30 min. Dissolved oxygen, salinity, and temperature levels were monitored during each experimental trial with a water quality meter (model 85; YSI Inc., Yellow Springs, OH) to ensure that the tank conditions remained comparable to those in PKD Bay.

After a 48-h acclimation period, sharks were implanted with an accelerometer transmitter as described above and given at least six hours to recover in the tank. Following the recovery period, an omnidirectional hydrophone (Model: VH165; Vemco Division, AMIRIX Systems Inc., Halifax, Nova Scotia) linked to a receiver (Model: VR100; Vemco Division, AMIRIX Systems Inc., Halifax, Nova Scotia) was used to record transmitted ODBA values corresponding to three biological activity states: resting, low activity, and high activity (O'Toole et al. 2010; Murchie et al. 2011). These three states were identified based on observations of juvenile sand tiger behavior in the same holding tank during a study investigating the physiological effects of capture and post-release recovery (Kneebone et al. 2013).

ODBA values corresponding to periods when sharks remained motionless (i.e., while buccal pumping) on the bottom of the tank were classified as resting. Slow swimming around the tank was classified as low activity; this was the most common behavior observed in this tank (Kneebone et al. 2013). During the early stages of the calibration experiment, we observed that the accelerometer sensor would log the maximum value after only one burst lasting from 1 to 3 s (i.e., the transmitted acceleration was always 3.463  $\text{m s}^{-2}$  no matter how many bursts were exhibited over the sampling interval). Therefore, to document acceleration values corresponding to high

activity, sharks were either: 1) chased until they burst swam, or 2) chased continuously for the ~55 s sampling interval if burst swimming did not occur. Treatment (2) was performed to establish the acceleration values that were representative of swimming at a faster pace than the slow swimming commonly observed (i.e., the low activity state) for the duration or a portion of the transmitter sampling interval. Data from each trial were pooled to examine the range of acceleration values representative of each activity level (Table 1). Both sharks were released back into PKD Bay following the calibration experiment and were monitored as part of the broader study.

#### Data processing and activity state classification

Prior to analysis, all transmitter data were examined individually and false detections rejected using criteria established by the tag manufacturer (Vemco; Pincock 2012). Detections collected within 24 h of release were also excluded to account for aberrant behavioral changes associated with the tagging process (O'Toole et al. 2010; Kneebone et al. 2013).

Rather than model ODBA values directly, each acceleration detection was classified into one of two activity states based on the results of the calibration experiment. As described above, the calibration experiments suggested that acceleration data could potentially be divided into three states corresponding to resting, slow swimming, and active/burst swimming behaviors. However, due to the low frequency of resting behavior in the wild (see [Results](#) section) we had limited interest in distinguishing between periods of resting and slow swimming behaviors, and so chose to assume two activity states: one corresponding to low activity (i.e., resting or slow swimming) and one corresponding to more active movements that would be associated with foraging or escape responses (hereafter referred to as

high activity). Because acceleration data are strictly positive, accelerations corresponding to both the low and high activity states were assumed to follow a gamma distribution (Bolker 2008). Two separate gamma distributions (parameterized in terms of shape and scale parameters) were fitted to low and high activity observations from the calibration experiment and were used as the basis for assigning each detected acceleration to the most probable activity state.

Trends in vertical movements were also examined as a second measure of activity. Tagging data obtained from sand tigers indicates the species is primarily benthic, spending the majority of its time at depth (Otway and Ellis 2011; Smale et al. 2012; Kneebone et al. 2014; Teter et al. 2015). However, movements to the surface have been previously documented, including within PKD Bay (Kneebone et al. 2014). Water depths in areas of receiver coverage in PKD Bay were generally >1.5 m (i.e., greater than one body length of the tagged sharks); thus, we considered off-bottom movements to the surface (depth < 0.50 m) as indicators of active swimming and a reasonable secondary proxy for animal activity. We ultimately chose to model the probability of a surface detection rather than raw depth due to the complex bathymetry and large tidal amplitude in PKD Bay, which would influence raw depth measurements irrespective of animal activity.

#### Identifying trends in activity using geostatistical mixed effects models

Our goal was to identify relationships between environmental covariates and activity patterns of juvenile sand tigers, and so we focused only on characterizing the probability of high activity given that a tagged individual was detected (i.e. we do not include a model for the probability of detection). We modeled the activity state

**Table 1** Range of overall dynamic body acceleration values ( $\text{m s}^{-2}$ ) corresponding to three activity levels observed during two accelerometer calibration experiments

Activity level	ST1108 (82 cm female)	ST1115 (97 cm male)	Combined
Resting	0.041–0.054 (0.044 ± 0.006)	0.068–0.109 (0.089 ± 0.014)	0.041–0.109 (0.075 ± 0.026)
Low activity	0.217–0.557 (0.420 ± 0.123)	0.122–0.462 (0.235 ± 0.117)	0.122–0.557 (0.355 ± 0.149)
High activity	0.788–3.463 (1.557 ± 0.804)	1.101–3.463 (1.747 ± 0.732)	0.788–3.463 (1.652 ± 0.752)

3.463  $\text{m s}^{-2}$  is the maximum capability of the V9AP acceleration sensor

Mean and standard deviation of the observed values are indicated in parentheses

of each observed detection as the outcome of a Bernoulli random variable (0 = low activity; 1 = high activity):

$$y_i \sim \text{Bernoulli}(p_i),$$

where  $p_i$  is the probability that detection  $i$  corresponds to the high activity state. The probability that a given detection corresponds to high activity can be modeled as a function of environmental covariates, as well as individual- or receiver-specific covariates as:

$$\text{logit}(p_i) = \beta_0 + \boldsymbol{\beta} \mathbf{X}_i,$$

where  $\beta_0$  is an intercept term representing the mean probability of a high activity detection,  $\boldsymbol{\beta}$  represents the vector of regression coefficients related to each included covariate, and  $\mathbf{X}_i$  is a vector of covariates specific to each detection. We discuss the rest of the analysis in terms of activity states, but we used the same approach to identify relationships between environmental drivers and the probability that a logged detection occurred at the surface (0 = below surface detection; 1 = surface detection).

To assess trends in activity related to environmental covariates, we incorporated water temperature, hour of the day, lunar phase, and tide stage as predictors of  $p_i$ . Water temperature for each acceleration detection was assigned based on ambient conditions measured by the data logger that was closest to the location of the detecting receiver in both space and time. Lunar phase (i.e. new, waxing, full, waning) was assigned using the ‘lunar’ package (Lazaridis 2014) in R (R Core Team 2016). Tide stage (i.e. ebb, low, flood, or high) was assigned to each detected acceleration using data for PKD Bay obtained from [http://tbone.biol.sc.edu/tide/sites\\_useastupper.html](http://tbone.biol.sc.edu/tide/sites_useastupper.html). Based on observations of tidal water flow in PKD Bay (J. Kneebone, pers. obs.), high and low tide were defined as the period encompassing 90 min before and after the timing of mean high and low water, respectively. As defined, each tidal stage had an approximately 3-h period. Covariates were screened for multicollinearity prior to model fitting. The full linear predictor for  $p_i$  was specified as a function of environmental covariates as:

$$\begin{aligned} \text{logit}(p_i) = & \beta_0 + \beta_1 \text{Temp}_i + \beta_2 \text{Temp}_i^2 + \beta_3 \sin\left(\frac{2\pi h_i}{24}\right) + \\ & \beta_4 \cos\left(\frac{2\pi h_i}{24}\right) + \beta_{5,6,7} \text{Tide}_i + \beta_{8,9,10} \text{Moon}_i, \end{aligned}$$

where the intercept term,  $\beta_0$ , corresponds to low tide and the new moon;  $\beta_1$  and  $\beta_2$  to a quadratic effect of water temperature (which allows for a non-linear relationship

with activity state);  $\beta_3$  and  $\beta_4$  to the trigonometric functions for hour of the day,  $h$ ;  $\beta_{5,6,7}$  to ebb, flood, and high tide; and  $\beta_{8,9,10}$  to waxing, full, and waning moon phases, respectively.

The above formulation implies that the probability of a high activity detection at a given receiver is independent of those at all other receivers and is constant between individuals. Given variation in local conditions that is not accounted for by the above covariates (e.g., depth, bottom type, prey densities), we expected that trends in activity at a given receiver would be more similar to those at neighboring receivers than those located further apart (Winton et al. 2018). To allow for spatial correlation between receivers,  $r$ , the above model was extended using a Gaussian random field (GRF),  $\Omega$ , (Lindgren et al. 2011; Thorson et al. 2015, 2017):

$$\text{logit}(p_i) = \beta_0 + \boldsymbol{\beta} \mathbf{X}_i + \Omega(r_i),$$

Here  $\Omega$  denotes the GRF allowing for spatial variation in the expected activity state, which we assumed follows a multivariate normal distribution:  $\Omega \sim \text{MVN}(0, \sigma_\Omega^2 \mathbf{C}_d)$ , where  $\sigma_\Omega^2$  is the marginal variance of  $\Omega$ .  $\mathbf{C}_d$  is the spatial correlation function between locations separated by a Euclidean distance of  $d$  (here specified as a Matérn function with a smoothness parameter,  $\nu$ , equal to 1 and a scaling parameter,  $\kappa$ , which was estimated following Lindgren et al. 2011). These two terms represent the spatial covariance among locations, which we assumed to be equal in both the north-south and east-west directions (i.e., isotropic). The correlation range (i.e. the distance at which observations can be considered independent),  $\rho$ , was calculated as the distance at which the correlation declines to approximately 10%, which was empirically derived as  $\sqrt{8}/\kappa$  following Lindgren et al. (2011).

Juvenile sand tigers exhibit site fidelity (Kneebone et al. 2012), and so we also expected that the activity states of an individual shark at a given receiver would be more similar than those logged at the same receiver by a different tagged individual. To account for autocorrelation related to differences in the distribution of individual sharks, the above spatial model was extended with a second GRF representing variation in  $\Omega$  for each tagged shark,  $s$ , denoted by  $\mathbf{E}_s$ :

$$\text{logit}(p_{i,s}) = \beta_0 + \boldsymbol{\beta} \mathbf{X}_i + \Omega(r_i) + \mathbf{E}_s(r_i),$$

where, as for  $\Omega$ ,  $\mathbf{E}_s$  was assumed to follow a multivariate normal distribution with mean zero and spatial covariance

given by  $\sigma_E^2 \mathbf{C}_d$ . The above model formulation implies that the correlation distance was stationary and did not vary between individuals. Here,  $\Omega$  accounts for spatial correlation common to all individuals that was not accounted for by the included covariates, and  $\mathbf{E}_s$  represented differences in the spatial correlation structure between individuals (Thorson et al. 2017); in statistical terms,  $\Omega$  represents the marginal spatial correlation field integrated over all individuals. In other words, individual variations were represented as differences from the overall spatial field ( $\Omega$ ), where the spatial random fields for individual sharks were assumed to be independent.

#### Parameter estimation, spatial prediction, and model selection

We treated variations in space and among individuals as random effects, which were estimated using a stochastic partial differential equation approximation to a Gaussian random field (Lindgren et al. 2011). The approach approximates a continuous Gaussian field using a computationally efficient Gaussian Markov random field approximation, which is defined over the region of interest on a triangulated mesh (Lindgren et al. 2011). To calculate the mesh and the sparse matrices used for this approximation, we used the R-INLA software (Lindgren et al. 2011; Lindgren and Rue 2015). Receiver locations were specified as the mesh nodes, and the coastline was specified as the mesh boundary. Fixed effects parameters were estimated via non-linear optimization of the maximum marginal likelihood using the R package Template Model Builder (Kristensen et al. 2016), which integrates across random effects using the Laplace approximation. The estimated fixed and random effects were then used to predict the distribution and probability of surface or high activity throughout the study area. We refer interested readers to Lindgren et al. (2011), Lindgren and Rue (2015), Thorson et al. (2015), and Kristensen et al. (2016) for further details regarding the statistical theory, spatial approximation, and computational approaches underlying the models used. Code for fitting the models described will be made available as part of the R package ‘TelemetrySpace’ on the second author’s publicly available GitHub page (<https://github.com/meganwinton/TelemetrySpace>).

Given the large number of detections available, we used the Bayesian information criterion (BIC; Schwarz 1978) for model selection. When sample sizes are large,

use of the more commonly applied Akaike information criterion (AIC; Akaike 1973) can result in overfitting (Zhu et al. 2009). The BIC is a likelihood-based model selection tool that is analogous to AIC but imposes a larger penalty for the number of parameters included and hence tends to result in a more parsimonious model (Bolker 2008). The BIC was calculated as:

$$\text{BIC} = -2^* nLL + k^* \ln(n),$$

where  $nLL$  is the negative log likelihood,  $k$  is the number of parameters, and  $n$  is the number of detections. Fixed effects terms were retained in the model if their inclusion resulted in lower BIC values. We used the selected model to predict the residual spatial variation (i.e. the variation not explained by the selected covariates) by setting the coefficients for all fixed effects other than the intercept term to zero (Thorson et al. 2017). Predicted values for the latent spatial and individual random fields were projected over PKD Bay using functions in the R-INLA package (Lindgren and Rue 2015).

## Results

The eight tagged juvenile sand tigers were monitored in PKD Bay for periods of seven to 78 days ( $47 \pm 28$  days; Mean  $\pm$  SD; Table 2). Detection data were obtained from all acoustic receivers except a single receiver that was lost prior to the first download period (Station 31; Table 3; Fig. 1). Recorded ODBA values spanned the extent of the acceleration sensor’s capabilities and the range of values recorded during the calibration experiment (Tables 1, 2; Fig. 2a). Six of the eight sharks showed evidence of resting or stationary behavior ( $\text{ODBA} \leq 0.109 \text{ m s}^{-2}$ ; Table 1; Fig. 2a) at various times during their monitoring periods, although the overall frequency of these events was very low ( $n = 73$ , 0.2%; Fig. 2a). Sharks were detected from the surface (0 m) to depths of 21.10 m; the mean depth of each shark ranged from 1.56–2.88 m throughout the full monitoring period (Fig. 2b; Table 2). Water temperature at the time and location of all acoustic detections ranged from 12.40–30.05 °C ( $19.97 \pm 2.26$  °C; Table 3).

The number of detections classified as high activity or surface detections varied considerably among individuals as well as among receivers (Tables 2, 3). Based

**Table 2** Summary of detection data obtained from juvenile sand tigers tagged with acoustic transmitters in Plymouth, Kingston, Duxbury (PKD) Bay, Massachusetts, during 2011

Shark	Sex	FL (cm)	Detection date	Days detected	Acceleration ( $\text{m s}^{-2}$ ) detections			Depth (m) detections			
					First	Last	Low activity	High activity	Range (Mean ± SD)	At Depth	Surface
ST1108	F	82	7/10/2011	9/30/2011	73	1303	59 (4%)	0.054–1.711 (0.279 ± 0.151)	1249	85 (6%)	0.00–9.67 (2.39 ± 1.40)
ST1109	F	104	7/12/2011	7/20/2011	8	309	3 (1%)	0.081–0.611 (0.184 ± 0.077)	293	0 (0%)	0.88–13.19 (2.88 ± 1.55)
ST1111	F	94	7/12/2011	7/19/2011	7	97	2 (2%)	0.122–1.331 (0.194 ± 0.149)	103	6 (6%)	0.00–5.06 (2.33 ± 1.17)
ST1112	M	96	7/12/2011	9/5/2011	55	9493	479 (5%)	0.068–3.463 (0.318 ± 0.212)	9859	114 (1%)	0.20–10.10 (2.59 ± 1.04)
ST1113	F	95	7/12/2011	9/8/2011	56	2426	733 (23%)	0.095–3.463 (0.458 ± 0.254)	2790	384 (12%)	0.00–7.47 (2.14 ± 1.44)
ST1114	M	108	7/16/2011	8/16/2011	31	1826	167 (8%)	0.081–2.553 (0.305 ± 0.185)	1757	256 (13%)	0.00–21.10 (1.56 ± 1.39)
ST1115	M	97	7/19/2011	10/5/2011	78	4527	487 (10%)	0.068–3.463 (0.355 ± 0.205)	4363	587 (12%)	0.00–8.57 (1.90 ± 1.24)
ST1116	F	85	7/18/2011	10/6/2011	68	7204	557 (7%)	0.122–3.463 (0.338 ± 0.242)	7365	344 (4%)	0.00–10.80 (2.16 ± 1.19)

The percentage of high activity and surface detections are presented in parentheses for each shark FL – fork length

on the fitted gamma distributions (low activity: shape = 1.75, scale = 0.10; high activity: shape = 4.96, scale = 0.29; Fig. 3), 2487 of the 29,672 acceleration detections (8.4%) were classified as high activity. A total of 1776 depth detections (6.0%) were classified as surface detections (<0.50 m).

#### Trends in activity and surface detections

While the probability of a high activity or surface detection was relatively low overall, the selected models indicated there was a relationship between each activity metric and lunar phase and hour of the day (Table 4). The estimated relationships suggested that juvenile sand tigers were more active (as defined relative to the estimated intercept value) at night between the hours of 15:00 and 02:00 and more likely to be detected at the surface between 17:00 and 04:00 h (Figs. 4, 5a). In comparison to the reference condition (i.e. new moon), the probability of both a high activity or a surface detection was lower during the other moon phases, and lowest during the waning moon (Table 5). There was also evidence that water temperature influenced the probability of a surface, though not a high activity, detection, with surface detections more likely at higher temperatures (Fig. 5b).

The residual spatial fields for both selected models indicated that the included covariates did not fully explain the observed variation, though the variability was better explained in some regions than in others (Fig. 6). High activity detections were more likely than predicted by the included covariates near the mouth through the southwestern side of the bay (near receivers 23–28 in Fig. 1) and less likely in the northern regions of the bay, which is predominantly shallow tidal marsh (Fig. 6a). Surface detections were more likely than predicted from the center into the western portion of the bay (near receivers 19, 20, and 21 in Fig. 1) and less likely to the north (Fig. 6b). While the probability of surface detections was highest in the area that was most frequented by tagged individuals (e.g., near receivers 20 and 21 in Fig. 1), high activity detections were most likely at locations that weren't often visited (Table 3). The estimated spatial range for both models (Table 5) implied that the spatial dependence between both high activity and surface detections was approximately 3000 m, or roughly one-third the length and one-half the width of PKD Bay. The predicted residual variation suggested that unmeasured covariates influenced the probability of both high activity and surface detections.

**Table 3** Summary of detection data obtained for acoustic transmitters from the array of 34 acoustic receivers deployed in Plymouth, Kingston, Duxbury Bay in 2011

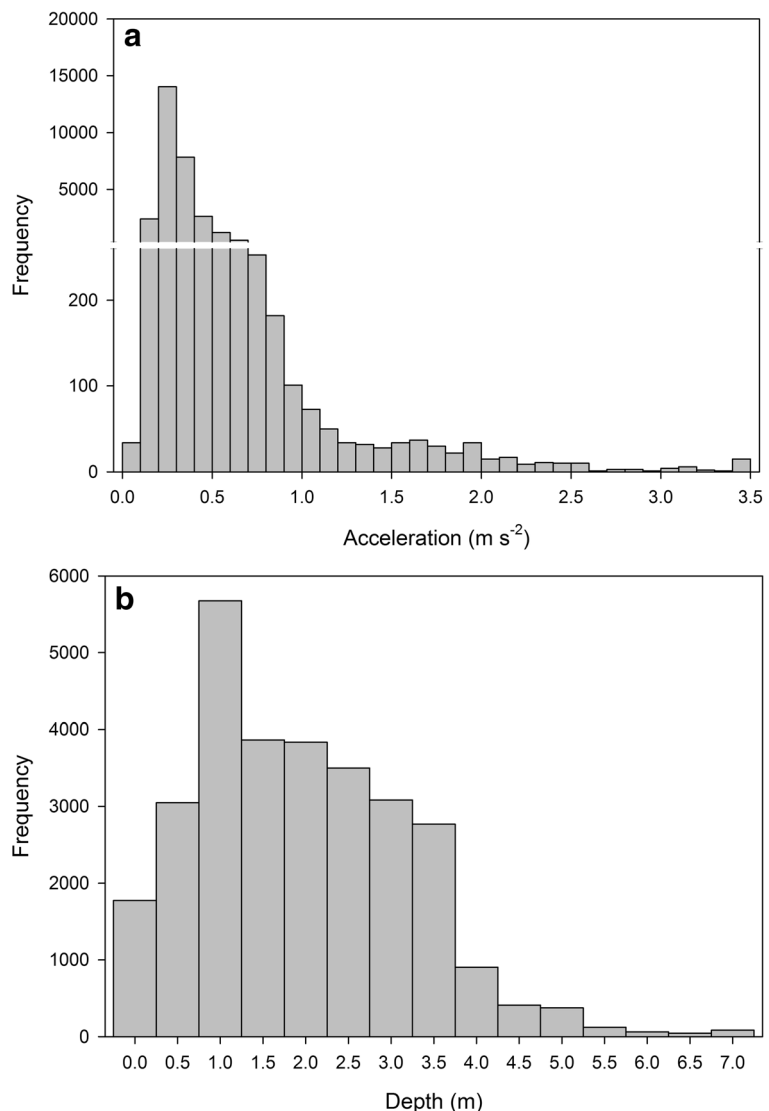
Station	Acceleration detections			Depth detections		Temperature range (°C)
	Total	Low activity	High activity	At Depth	Surface	
1	207	193	14 (7%)	190	15 (7%)	16–24 (19)
2	2258	2106	152 (7%)	2126	107 (5%)	13–28 (20)
3	3335	3118	217 (7%)	3171	113 (3%)	12–29 (20)
4	16	13	3 (19%)	17	1 (6%)	14–18 (17)
5	377	354	23 (6%)	406	4 (1%)	13–27 (21)
6	2062	1979	83 (4%)	1933	41 (2%)	13–25 (20)
7	4043	3843	200 (5%)	4009	79 (2%)	12–30 (20)
8	1790	1687	103 (6%)	1791	18 (1%)	12–29 (20)
9	480	463	17 (4%)	469	3 (1%)	13–28 (21)
10	2451	2363	88 (4%)	2373	72 (3%)	12–26 (20)
11	358	342	16 (4%)	355	0 (0%)	12–27 (21)
12	383	350	33 (9%)	388	11 (3%)	14–25 (21)
13	56	53	3 (5%)	56	1 (2%)	14–28 (18)
14	54	52	2 (4%)	44	2 (4%)	16–25 (20)
15	33	32	1 (3%)	27	0 (0%)	16–25 (19)
16	138	82	56 (41%)	146	0 (0%)	16–24 (18)
17	7	6	1 (14%)	9	0 (0%)	16–23 (18)
18	77	56	21 (27%)	93	0 (0%)	16–19 (17)
19	33	31	2 (6%)	24	1 (4%)	14–22 (18)
20	2773	2375	398 (14%)	2275	514 (18%)	13–27 (19)
21	2988	2699	289 (10%)	2555	408 (14%)	12–27 (20)
22	5081	4462	619 (12%)	4703	344 (7%)	12–29 (20)
23	438	351	87 (20%)	411	35 (8%)	13–25 (19)
24	68	28	40 (59%)	63	3 (5%)	16–28 (19)
25	16	14	2 (13%)	8	3 (27%)	16–25 (18)
26	6	3	3 (50%)	9	0 (0%)	17–24 (18)
27	17	13	4 (24%)	14	0 (0%)	13–23 (17)
28	5	5	0 (0%)	7	0 (0%)	17–23 (18)
29	33	30	3 (9%)	24	0 (0%)	14–24 (18)
30	64	61	3 (5%)	62	0 (0%)	13–26 (18)
31	Receiver lost: No data recovered					
32	2	1	1 (50%)	2	0 (0%)	17–20 (18)
33	6	4	2 (33%)	6	0 (0%)	15–20 (17)
34	17	16	1 (6%)	13	1 (7%)	15–19 (17)

Percentages in parentheses represent the percent of total detections in that category. Mean temperature is presented in parentheses

The patterns described above were consistent among all eight tagged sharks, but the estimated variance of the spatial random effects indicated greater variation in the individual than the ‘overall’ spatial field for both activity

metrics (Table 5; Figs. 7, 8). In other words, some sharks spent more time in the high activity state or near the surface than others and vice-versa. For example, variation in the spatial fields of ST1113, ST115, and ST1116

**Fig. 2** Frequency histogram of juvenile sand tiger (a) acceleration ( $\text{m s}^{-2}$ ) and (b) depth (m) data collected in Plymouth, Kingston, Duxbury Bay. Note the break in the y-axis in (a). Ten depth observations from 7 to 22 m were recorded but are not presented in (b) due to their relatively low frequency of occurrence



suggested that these individuals were more active than the other tagged sharks over a broader area (Fig. 7). Based on the individual spatial fields, most tagged sharks (ST1108, ST1109, ST1112, ST1113, ST1114, ST1115) were more likely to be detected at the surface along the western edge of the bay. In contrast to the other individuals, ST1111 logged more surface detections than expected in the middle of the bay, and ST1116 logged more along the northern edge of the bay (Fig. 8).

## Discussion

In this study, we directly measured the activity of eight juvenile sand tigers in a seasonal nursery area using

acoustic transmitters incorporating accelerometers. Acceleration and depth data indicated that tagged sand tigers spent most of their time at depth in the 'low' activity state while in PKD Bay. This observation corroborates previous general descriptions that sand tigers are sluggish, slow-swimming, demersal fish (Compagno 2001; Collette and Klein-MacPhee 2002), as well as numerous underwater observations of activity (e.g., Otway et al. 2003; Smith et al. 2015).

Descriptive accounts have commonly reported that sand tigers are 'more active' (e.g., Pollard et al. 1996; Compagno 2001; Collette and Klein-MacPhee 2002; Smale 2005) and more willing to take baits (Bigelow and Schroeder 1953) at night, which suggests that the diel trends in high activity and surface detections

**Fig. 3** Histogram of overall dynamic body acceleration and observed activity states during the transmitter calibration experiment. The blue dashed line corresponds to the estimated gamma distribution for the low activity state, and the red line to that for the high activity state. The fitted distributions were used as the basis for assigning each acceleration logged in PKD Bay to the most probable activity state

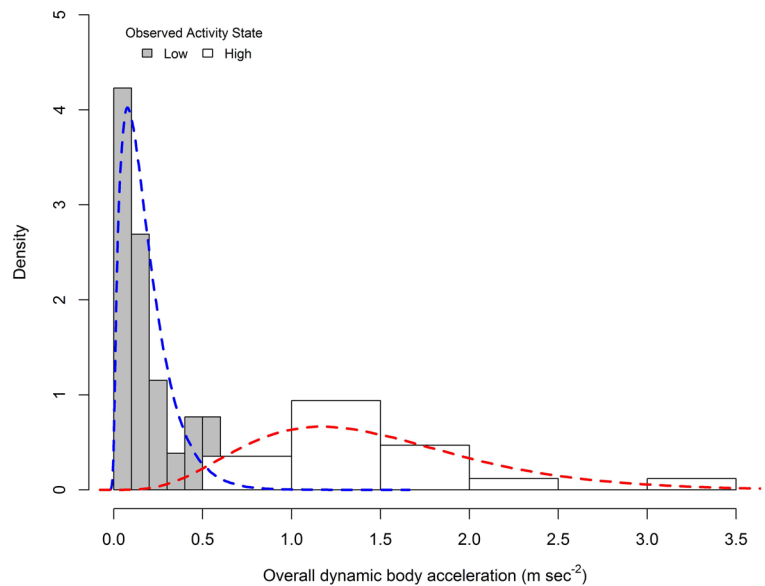


**Table 4** Relative goodness of fit for candidate models estimating the probability that a juvenile sand tiger detection corresponds to a high activity or a surface detection

Fixed effects parameters	<i>k</i>	High Activity		Surface	
		<i>nLL</i>	<i>BIC</i>	<i>nLL</i>	<i>BIC</i>
$\beta_0$	4	8545	17,132	6715	13,472
$\beta_0 + \beta_{5, 6, 7}\text{Tide}$	7	7906	15,883	5835	11,743
$\beta_0 + \beta_{8, 9, 10}\text{Moon}$	7	7889	15,851	5695	11,462
$\beta_0 + \beta_1\text{Temp}$	5	7909	15,869	5773	11,597
$\beta_0 + \beta_1\text{Temp} + \beta_2\text{Temp}^2$	6	7903	15,867	5769	11,600
$\beta_0 + \beta_3\sin\left(\frac{2\pi\text{hour}}{24}\right) + \beta_4\cos\left(\frac{2\pi\text{hour}}{24}\right)$	6	7872	15,806	5649	11,360
$\beta_0 + \beta_{5, 6, 7}\text{Tide} + \beta_{8, 9, 10}\text{Moon}$	10	7882	15,867	5689	11,481
$\beta_0 + \beta_1\text{Temp} + \beta_2\text{Temp}^2 + \beta_{5, 6, 7}\text{Tide}$	9	7894	15,880	5763	11,618
$\beta_0 + \beta_1\text{Temp} + \beta_{5, 6, 7}\text{Tide}$	8	7900	15,882	5767	11,616
$\beta_0 + \beta_3\sin\left(\frac{2\pi\text{hour}}{24}\right) + \beta_4\cos\left(\frac{2\pi\text{hour}}{24}\right) + \beta_{5,6,7}\text{Tide}$	9	7865	15,823	5643	11,379
$\beta_0 + \beta_1\text{Temp} + \beta_2\text{Temp}^2 + \beta_{8, 9, 10}\text{Moon}$	9	7884	15,860	5600	11,293
$\beta_0 + \beta_1\text{Temp} + \beta_{8, 9, 10}\text{Moon}$	8	7888	15,858	5608	11,299
$\beta_0 + \beta_3\sin\left(\frac{2\pi\text{hour}}{24}\right) + \beta_4\cos\left(\frac{2\pi\text{hour}}{24}\right) + \beta_{8,9,10}\text{Moon}$	9	<b>7851</b>	<b>15,794</b>	5507	11,107
$\beta_0 + \beta_1\text{Temp} + \beta_2\text{Temp}^2 + \beta_3\sin\left(\frac{2\pi\text{hour}}{24}\right) + \beta_4\cos\left(\frac{2\pi\text{hour}}{24}\right)$	8	7858	15,798	5573	11,229
$\beta_0 + \beta_1\text{Temp} + \beta_3\sin\left(\frac{2\pi\text{hour}}{24}\right) + \beta_4\cos\left(\frac{2\pi\text{hour}}{24}\right)$	7	7865	15,801	5576	11,224
$\beta_0 + \beta_1\text{Temp} + \beta_3\sin\left(\frac{2\pi\text{hour}}{24}\right) + \beta_4\cos\left(\frac{2\pi\text{hour}}{24}\right) + \beta_{5,6,7}\text{Tide}$	10	7856	15,815	5569	11,242
$\beta_0 + \beta_1\text{Temp} + \beta_2\text{Temp}^2 + \beta_3\sin\left(\frac{2\pi\text{hour}}{24}\right) + \beta_4\cos\left(\frac{2\pi\text{hour}}{24}\right) + \beta_{5,6,7}\text{Tide}$	11	7849	15,812	5566	11,246
$\beta_0 + \beta_1\text{Temp} + \beta_{5, 6, 7}\text{Tide} + \beta_{8, 9, 10}\text{Moon}$	11	7880	15,873	5601	11,316
$\beta_0 + \beta_1\text{Temp} + \beta_2\text{Temp}^2 + \beta_{5, 6, 7}\text{Tide} + \beta_{8, 9, 10}\text{Moon}$	12	7875	15,874	5593	11,310
$\beta_0 + \beta_1\text{Temp} + \beta_3\sin\left(\frac{2\pi\text{hour}}{24}\right) + \beta_4\cos\left(\frac{2\pi\text{hour}}{24}\right) + \beta_{8,9,10}\text{Moon}$	10	7847	15,797	5410	10,924
$\beta_0 + \beta_1\text{Temp} + \beta_2\text{Temp}^2 + \beta_3\sin\left(\frac{2\pi\text{hour}}{24}\right) + \beta_4\cos\left(\frac{2\pi\text{hour}}{24}\right) + \beta_{8,9,10}\text{Moon}$	11	7842	15,797	<b>5404</b>	<b>10,921</b>
$\beta_0 + \beta_1\text{Temp} + \beta_3\sin\left(\frac{2\pi\text{hour}}{24}\right) + \beta_4\cos\left(\frac{2\pi\text{hour}}{24}\right) + \beta_{5,6,7}\text{Tide} + \beta_{8,9,10}\text{Moon}$	13	7839	15,812	5401	10,936
$\beta_0 + \beta_1\text{Temp} + \beta_2\text{Temp}^2 + \beta_3\sin\left(\frac{2\pi\text{hour}}{24}\right) + \beta_4\cos\left(\frac{2\pi\text{hour}}{24}\right) + \beta_{5,6,7}\text{Tide} + \beta_{8,9,10}\text{Moon}$	14	7834	15,812	5394	10,933

Models are ranked from least to most complex. The best fitting model for each activity metric is indicated in bold. *k*: number of parameters estimated, which includes three parameters corresponding to the spatial variance and correlation terms; *nLL*: negative log-likelihood; *BIC*: Bayesian Information Criterion

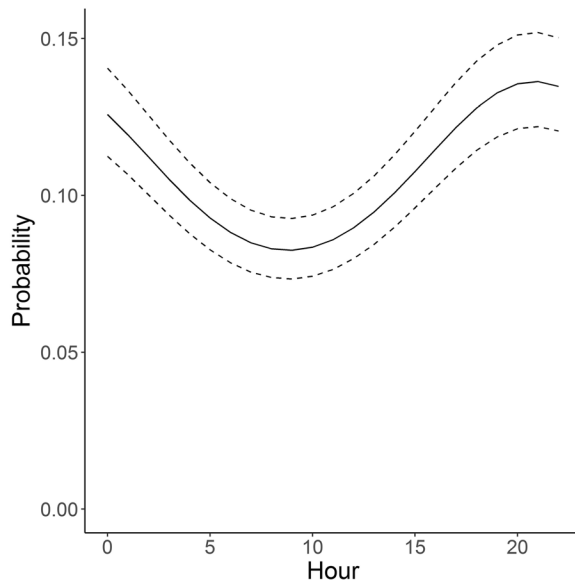


**Fig. 4** Probability of a high activity detection in relation to hour of the day based on the selected geostatistical mixed effects model. Dashed lines indicate the 95% confidence intervals

documented here may be related to foraging (Brewster et al. 2018). This assertion of increased nighttime foraging has also been inferred based on diel trends in short-term active and passive acoustic telemetry data collected from sand tigers off eastern Australia (Bruce et al. 2005). Robbins et al. (2013) reported that there was no significant difference in the rate of bait depredation by sand tigers

throughout the day (i.e., over a 24 h period), thereby suggesting that higher nighttime activity may be related to the search for prey rather than the consumption of it.

Throughout their residency in PKD Bay, juvenile sand tigers have been observed actively pursuing and feeding on menhaden schools (Kneebone et al. 2012), and shark movements and space use seem to be closely associated with menhaden distribution (J. Kneebone pers. obs). Thus, it is possible that the increased probability of high activity at less frequented locations (in terms of both detecting receivers as well as temperature and depth) was associated with short-term shifts in menhaden distribution into these areas. While we cannot rule out that a portion of the high activity detections observed were due to startle responses (i.e., resulting from environmental or anthropogenic disturbances), it seems reasonable to assume that such responses would occur rarely. Thus, the high activity state most likely corresponds to foraging given our observations of shark feeding activity in the bay.

In contrast to high activity detections, surface detections were more likely in a commonly-inhabited area along the western edge of PKD Bay and occurred more frequently at higher water temperatures (Figs. 5b, 6, 8). During their seasonal residency, tagged sand tigers spend the majority of their time in the western portion of PKD Bay (e.g., near receiver 20; Fig. 1), an area that is characterized by shallow (< 2.5 m), tidal flats that are

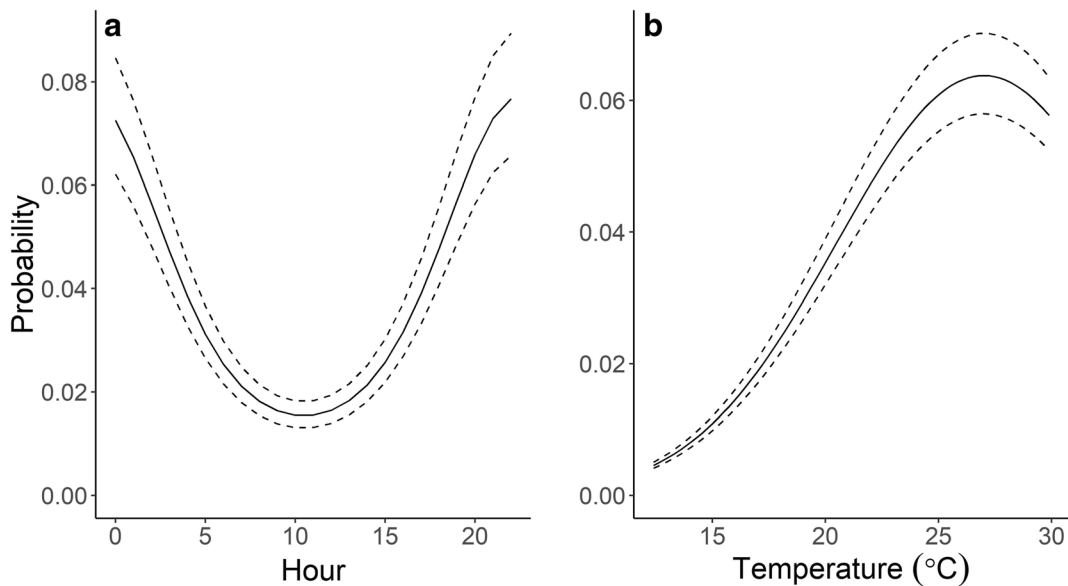


**Fig. 5** Probability of a surface detection in relation to hour of the day (a) and water temperature (b) based on the selected geostatistical mixed effects model. Dashed lines indicate the 95% confidence intervals. Note that the y-axis scale varies between panels

**Table 5** Estimated parameters and standard errors from a geostatistical mixed effects model fitted to detection data from eight juvenile sand tigers

Parameter	High Activity		Surface	
	Estimate	S.E.	Estimate	S.E.
Intercept ( $\beta_0$ )	-2.13	0.40	-3.33	0.45
Linear effect of temperature ( $\beta_1$ )	—	—	0.43	0.03
Quadratic effect of temperature ( $\beta_2$ )	—	—	-0.07	0.02
Sine component of daily trend ( $\beta_3$ )	0.24	0.03	0.83	0.05
Cosine component of daily trend ( $\beta_4$ )	-0.15	0.03	-0.12	0.04
Waxing moon ( $\beta_8$ )	-0.08	0.06	-0.36	0.06
Full moon ( $\beta_9$ )	-0.28	0.06	-1.18	0.09
Waning moon ( $\beta_{10}$ )	-0.40	0.07	-1.21	0.08
Marginal spatial standard deviation ( $\sigma_\Omega$ )	0.49	0.14	0.52	0.25
Marginal spatio-individual standard deviation ( $\sigma_E$ )	0.62	0.11	0.90	0.19
Spatial correlation range, $\rho$	3356 m	754 m	2659 m	743 m

Note that  $\rho$  was empirically derived as described in the text. Parameters follow those specified in the text. A dash indicates that the parameter was not included in the selected model for the specified activity metric

partially exposed at low tide and experience comparatively warm water temperatures (Table 3; Kneebone et al. 2012). Due to the water depth in this area, less vertical movement would be required to reach the surface; therefore, one would expect to observe a relatively high number of surface observations relative to other

deeper, colder locations. Shallow water depths near receiver 25 (Fig. 1) also likely contributed to the higher probability of surface detections in this area (Fig. 8). However, tide stage was not a predictor of surface detections, which suggests that these observations are indicative of presence at the surface and not swimming

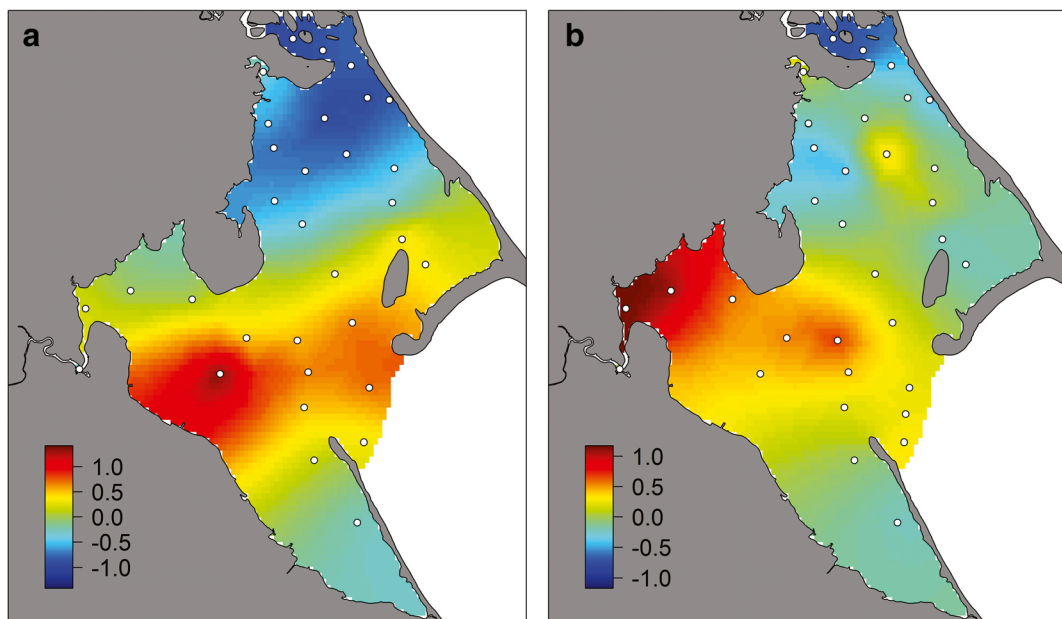


**Fig. 6** Residual variation in the probability of a high activity (a) or surface detection (b) for eight tagged juvenile sand tigers. The legend indicates the deviation from the mean predicted value at each site on the logit scale. Green areas (values closest to 0)

indicate areas where the observed values align with those predicted based on relationships with environmental covariates. Blue areas are those with lower values than would be expected, and the red regions are those with higher values

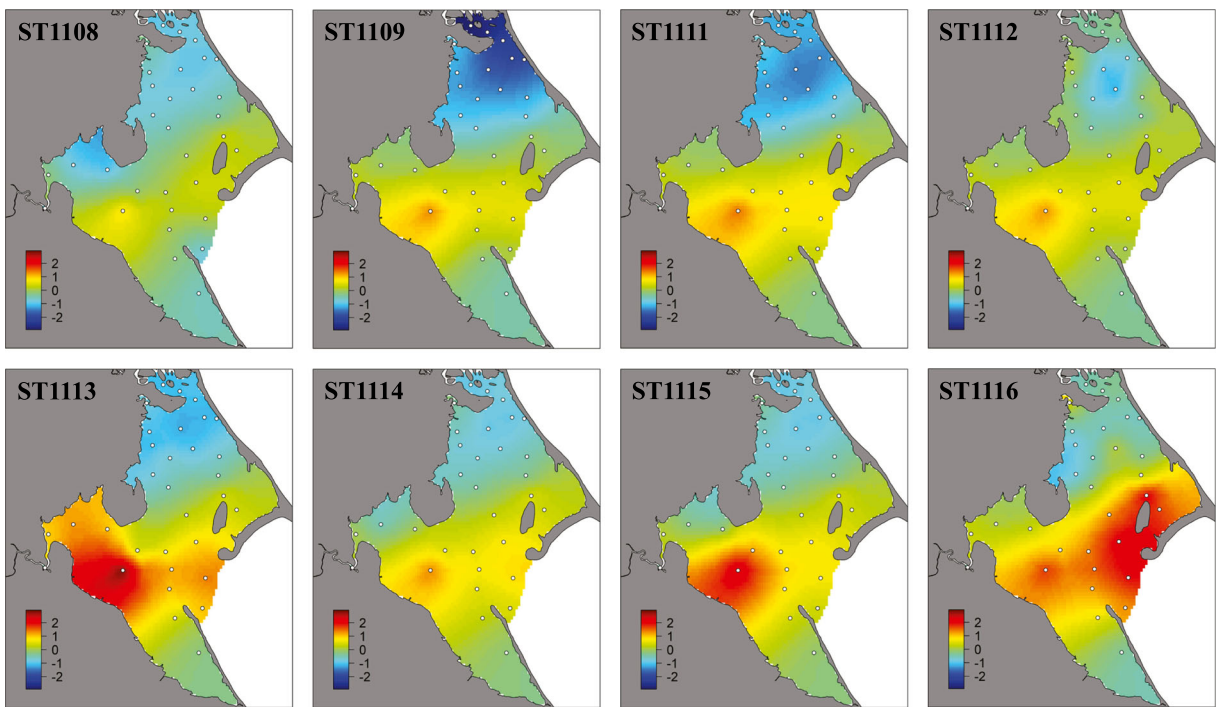


**Fig. 7** Individual residual variation in the probability of a high activity detection for eight tagged juvenile sand tigers. The legend indicates the deviation from the mean predicted value at each site on the logit scale. Green areas (values closest to 0) indicate areas

where the observed values align with those predicted based on relationships with environmental covariates. Blue areas are those with lower values than would be expected and red are those with higher values

in water depths <0.5 m, which could only occur within the apparent receiver detection ranges at low tide.

Other environmental factors, such as light intensity and substrate type, may also influence the diel activity patterns observed in PKD Bay (Reebs 2002; Hamilton et al. 2014). Unfortunately, detailed data on substrate type were not available for PKD Bay, which precluded our ability to examine its effect on sand tiger activity. Light intensity data were available for some regions of PKD Bay during the study period but were not included in the model due to our inability to account for fine-scale differences in light intensity throughout the receiver array (i.e., in response to weather conditions, local water depth, and local water turbidity). Regardless, light intensity at-depth in PKD Bay was generally highest during the mid-day hours (J. Kneebone, unpublished data) when the probability of high activity and surface detections were lowest. The potential influence of light on diel activity is further supported by the finding that the highest probability of high activity occurred during the new moon, a period characterized by no or low moonlight. This suggests that juvenile sand tigers may hunt more effectively in low ambient light, a scenario

that has been hypothesized for other aquatic species (Weltz et al. 2013; Gleiss et al. 2017).

It is important to note that our interpretation of juvenile sand tiger activity patterns is constrained by our classification scheme. We were interested in using ODBA as a proxy for juvenile sand tiger activity, and so imposed two activity states based on the results of the calibration experiment. This type of calibration approach has been used previously to link raw acceleration data to biologically-relevant behaviors/activity states (O'Toole et al. 2010; Murchie et al. 2011). It is possible that tank space constraints impacted the resulting distributions and classification of high activity detections during the calibration experiment, but the activity state-dependent distributions estimated from the calibration data did mirror the distribution of detections observed in the wild. Furthermore, given the low degree of overlap between the distributions for low and high activity states, the potential for gross misclassification of activity state seems low. In addition, it is possible that some of the surface detections occurred when individuals surfaced to swallow air, which is a behavior known to occur in sand tigers (Compagno 2001), albeit at an unknown frequency.

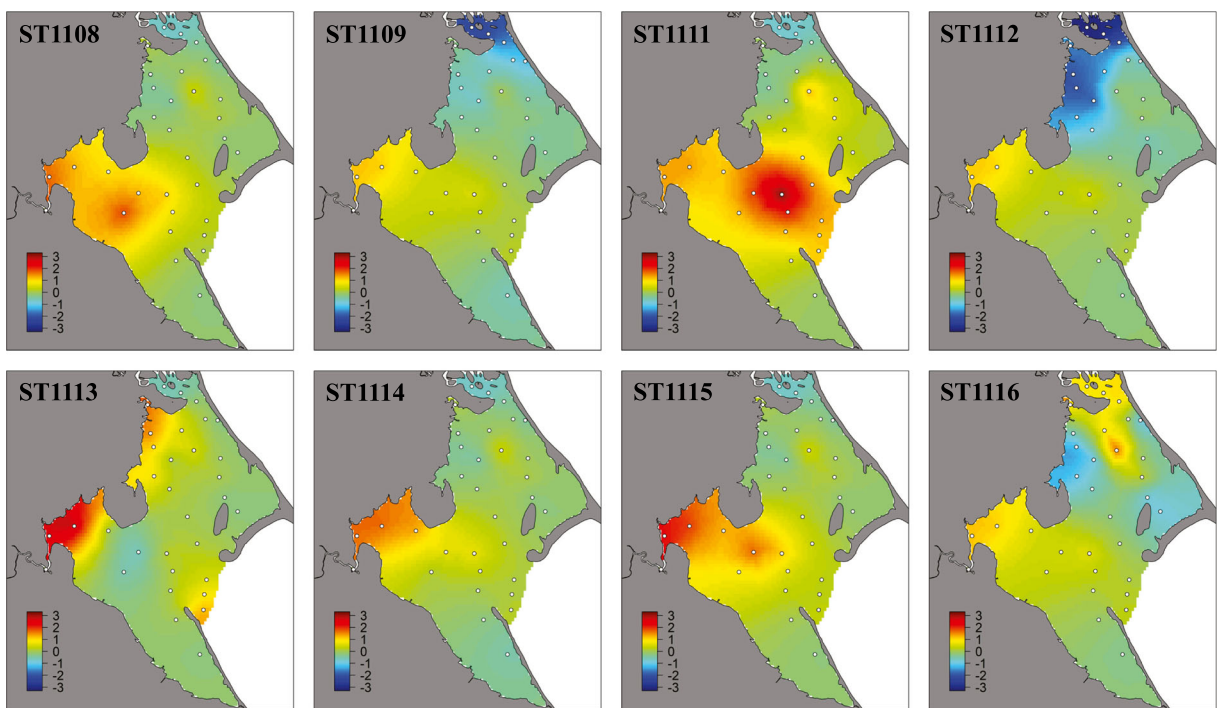


**Fig. 8** Individual residual variation in the probability of a surface detection for eight tagged juvenile sand tigers. The legend indicates the deviation from the mean predicted value at each site on the logit scale. Green areas (values closest to 0) indicate areas

where the observed values align with those predicted based on relationships with environmental covariates. Blue areas are those with lower values than would be expected and red are those with higher values

Similarly, the two activity states do not necessarily reflect the species' biology adequately or may reflect the biological reality of some individuals better than others. While there was only a 26 cm difference between the smallest and largest tagged individuals, it is plausible that shark activity patterns could be related to size. The calibration experiments were conducted using two individuals of similar size to other tagged individuals, but there was a large degree of individual variation in values logged in the field. By fitting our model with random effects for individual sharks, we were able to describe patterns of activity common to multiple individuals (McKellar et al. 2015). A more mechanistic understanding of the individual differences observed here (e.g., differences in acceleration related to size) would require a greater sample size but would potentially allow for better determination of activity states.

Given the ephemeral nature of feeding and other activities, it is likely that a large fraction of high activity events exhibited in PKD Bay were not recorded due to accelerometer transmission rates (which alternated between acceleration and depth and only transmitted every 60 to 90 s even when within range of a receiver). It is

also possible that the volume of data missing due to time periods when sharks were not within range of a receiver may have biased our results (Payne et al. 2010). Detection efficiency control experiments conducted in PKD Bay determined that detection ranges did not vary substantially during the time period monitored (J. Kneebone, unpubl. data), but the array did not provide full coverage of the bay. Future studies should seek to extend the models used here with a component explicitly accounting for variation in the detection process to address this potential source of bias (Pedersen and Weng 2013).

By applying a novel geostatistical modeling approach, we were able to quantify the influence of physical and environmental factors on juvenile sand tiger activity patterns at both a population- and individual-level. Unlike non-spatial generalized linear modeling approaches, which are commonly applied to infer relationships between acoustic detection data and environmental covariates (e.g., Simpfendorfer et al. 2011; Henderson et al. 2014), the models applied here account for the influence of unmeasured habitat variables via inclusion of spatial random effects, which act as an

“umbrella” term for spatially-varying covariates that are not included explicitly in the model structure (Thorson et al. 2017; Winton et al. 2018). In general, our model results corroborate previous descriptions of sand tiger activity patterns; however, the included covariates did not fully account for the observed variation in high activity and surface detections. While accelerometer transmitters cannot document the exact behavior of tagged animals in the wild, the geostatistical modelling approach provided a tool to better understand potential mechanisms underlying the observed variation, which would not have been apparent if analyzed in a non-spatial framework. Additional research is necessary to evaluate the activity patterns of sub-adult and adult sand tigers in other regions to determine if they exhibit similar activity patterns to juveniles within PKD Bay. Nonetheless, the trends in activity identified here may have implications for managing bycatch of this species in the U.S. Atlantic and beyond.

**Acknowledgements** We gratefully acknowledge Pine duBois and Alex Mansfield of the Jones River Environmental Heritage Center for providing the infrastructure for our holding tank and their logistical support, Barbara Bailey and Holly Bourbon for their assistance with the holding tank construction, Jay Hilliard and Dave Lindamood for enabling the initial documentation of sharks in PKD Bay, Donald Beers and the Duxbury Harbormaster’s Office for providing dockage, and Heather Hollema for her assistance with tagging and receiver maintenance. This research was funded by awards from the NOAA Proactive Conservation Program, the Sea World Conservation Society, and the Massachusetts Environmental Trust as well as support from the Federal Aid in Sportfish Restoration Act. This is Massachusetts Division of Marine Fisheries Contribution No. 99.

## References

- Akaike H (1973) Information theory as an extension of the maximum likelihood principle. In Petrov BN, Csaki F (eds) Second international symposium on information theory. Budapest, Hungary pp 267–281
- ASMFC (Atlantic States Marine Fisheries Commission) (2008) Interstate fishery management plan for Atlantic coastal sharks. ASMFC, Washington, DC 172pp
- Barnett A, Payne NL, Semmens JM, Fitzpatrick R (2016) Ecotourism increases the field metabolic rate of whitetip reef sharks. Biol Conserv 199:132–136
- Beck MW, Heck KL Jr, Able KW, Childers DL, Eggleston DB, Gillanders BM et al (2001) The identification, conservation, and management of estuarine and marine nurseries for fish and invertebrates: a better understanding of the habitats that serve as nurseries for marine species and the factors that create site-specific variability in nursery quality will improve conservation and management of these areas. Bioscience 51(8):633–641
- Bolker BM (2008) Ecological models and data in R. Princeton University Press, Princeton
- Bigelow HB, Schroeder WC (1953) Fishes of the Gulf of Maine. Fish Bull 53:74
- Brewster LR, Dale JJ, Guttridge TL, Gruber SH, Hansell AC, Elliott M, Cowx IG, Whitney NM, Gleiss AC (2018) Development and application of a machine learning algorithm for classification of elasmobranch behaviour from accelerometry data. Mar Biol 165(4):62
- Brodie S, Taylor MD, Smith JA, Suthers IM, Gray CA, Payne NL (2016) Improving consumption rate estimates by incorporating wild activity into a bioenergetics model. Ecol Evol 6(8): 2262–2274
- Brownscombe JW, Wilson AD, Samson E, Nowell L, Cooke SJ, Danylchuk AJ (2015) Individual differences in activity and habitat selection of juvenile queen conch evaluated using acceleration biologgers. Endanger Species Res 27(2):181–188
- Brownscombe JW, Cooke SJ, Danylchuk AJ (2017) Spatiotemporal drivers of energy expenditure in a coastal marine fish. Oecologia 183(3):689–699
- Bruce BD, Stevens JD, Bradford R (2005) Designing protected areas for grey nurse sharks off eastern Australia (p. 56). Hobart: CSIRO Marine and Atmospheric Research
- Burnett NJ, Hinch SG, Donaldson MR, Furey NB, Patterson DA, Roscoe DW, Cooke SJ (2014) Alterations to dam-spill discharge influence sex-specific activity, behaviour and passage success of migrating adult sockeye salmon. Ecohydrology 7(4):1094–1104
- Carlson JK, McCandless C, Cortés E, Grubbs RD, Andrews KI, MacNeil MA, Musick JA (2009) An update on the status of the sand tiger shark, *Carcharias taurus*, in the Northwest Atlantic Ocean. NOAA Tech Memorandum NMFS-SEFSC-585
- Castro J, Woodley CM, Brudek R (1999) A preliminary evaluation of the status of shark species. FAO Fisheries Technical Paper No. 380, FAO, Rome, 72pp
- Collette BB, Klein-MacPhee G (2002) Fishes of the Gulf of Maine, 3rd edn. Smithsonian Institute Press, Washington, DC, pp 25–27
- Compagno LJV (2001) Sharks of the World. FAO species catalogue for fishery purposes, No 1, vol 2. Food and Agriculture Organization of the United Nations, Rome 269 pp
- Gilmore RG, Dodrill JW, Linley PA (1983) Embryonic development of the sand tiger shark *Odontaspis taurus* (Rafinesque). Fish Bull 81:201–225
- Gleiss AC, Dale JJ, Holland KN, Wilson RP (2010) Accelerating estimates of activity-specific metabolic rate in fishes: testing the applicability of acceleration data-loggers. J Exp Mar Bio Ecol 385(1–2):85–91
- Gleiss AC, Wilson RP, Shepard EL (2011) Making overall dynamic body acceleration work: on the theory of acceleration as a proxy for energy expenditure. Methods Ecol Evol 2(1): 23–33
- Gleiss AC, Morgan DL, Whitty JM, Keleher JJ, Fossette S, Hays GC (2017) Are vertical migrations driven by circadian behaviour? Decoupling of activity and depth use in a large riverine elasmobranch, the freshwater sawfish (*Pristis pristis*). Hydrobiologia 787(1):181–191

- Hamilton SL, Smith JE, Price NN, Sandin SA (2014) Quantifying patterns of fish herbivory on Palmyra atoll (USA), an uninhabited predator-dominated Central Pacific coral reef. *Mar Ecol Prog Ser* 501:141–155
- Heithaus MR (2007) Nursery areas as essential shark habitats: a theoretical perspective. In: McCandless CT, Kohler NE, Pratt HL Jr (eds) *Shark nursery grounds of the Gulf of Mexico and east coast waters of the United States*. American Fisheries Society, Bethesda, MD, p 3–13.
- Henderson MJ, Fabrizio MC, Lucy JA (2014) Movement patterns of summer flounder near an artificial reef: effects of fish size and environmental cues. *Fish Res* 153:1–8
- Heupel MR, Semmens JM, Hobday AJ (2006) Automated acoustic tracking of aquatic animals: scales, design, and deployment of listening station arrays. *Mar Freshw Res* 57:1013–1020
- Heupel MR, Carlson JK, Simpfendorfer CA (2007) Shark nursery areas: concepts, definition, characterization and assumptions. *Mar Ecol Prog Ser* 337:287–297
- Iwanowicz HR, Anderson RD, Ketschke BA (1974) A study of the marine resources of Plymouth, Kingston, and Duxbury Bay. Monograph Series Number 17. Division of Marine Fisheries, Boston, p 37
- Kahle D, Wickham H (2013) ggmap: spatial visualization with ggplot2. *R J* 5(1):144–161
- Kneebone J, Chisholm J, Skomal GB (2012) Seasonal residency, habitat use, and site fidelity of juvenile sand tigers *Carcharias taurus* in a Massachusetts estuary. *Mar Ecol Prog Ser* 471:165–185
- Kneebone J, Chisholm J, Bernal D, Skomal GB (2013) The physiological effects of capture stress, recovery, and post-release survivorship of juvenile sand tigers (*Carcharias taurus*) caught on rod and reel. *Fish Res* 147:103–114
- Kneebone J, Chisholm J, Skomal G (2014) Movement patterns of juvenile sand tigers (*Carcharias taurus*) along the east coast of the USA. *Mar Biol* 161(5):1149–1163
- Knip DM, Heupel MR, Simpfendorfer CA (2010) Sharks in nearshore environments: models, importance, and consequences. *Mar Ecol Prog Ser* 402:1–11
- Kolarevic J, Aas-Hansen Ø, Espmark Å, Baeverfjord G, Terjesen BF, Damsgård B (2016) The use of acoustic acceleration transmitter tags for monitoring of Atlantic salmon swimming activity in recirculating aquaculture systems (RAS). *Aquac Eng* 72:30–39
- Kristensen K, Nielsen A, Berg CW, Skaug H, Bell BM (2016) TMB: automatic differentiation and Laplace approximation. *J Stat Softw* 70:1–21
- Lazaridis E (2014) Lunar: lunar phase & distance, seasons and other environmental factors (version 0.1-04). Available from <http://statistics.lazaridis.eu>
- Lear KO, Whitney NM, Brewster LR, Morris JJ, Hueter RE, Gleiss AC (2016) Correlations of metabolic rate and body acceleration in three species of coastal sharks under contrasting temperature regimes. *J Exp Biol* 220:397–407
- McKellar AE, Langrock R, Walters JR, Kesler DC (2015) Using mixed hidden Markov models to examine behavioral states in a cooperatively breeding bird. *Behav Ecol* 26(1):148–157
- Lindgren F, Rue H (2015) Bayesian spatial modelling with R-INLA. *J Stat Softw* 63:1–25
- Lindgren F, Rue H, Lindstrøm J (2011) An explicit link between Gaussian fields and Gaussian Markov random fields: the stochastic partial differential equation approach. *J R Stat Soc Ser B Stat Methodol* 73:423–498
- McLusky DS, Elliott M (2004) *The estuarine ecosystem: ecology, threats and management*. 3<sup>rd</sup> Edition. Oxford University Press
- Murphy KJ, Cooke SJ, Danylchuk AJ, Suski CD (2011) Estimates of field activity and metabolic rates of bonefish (*Albula vulpes*) in coastal marine habitats using acoustic tri-axial accelerometer transmitters and intermittent-flow respirometry. *J Exp Mar Biol Ecol* 396(2):147–155
- Musick JA, Branstetter S, Colvocoresses JA (1993) Trends in shark abundance from 1974 to 1991 for the Chesapeake bight region of the U.S. mid-Atlantic Coast. NOAA Technical Report NMFS 115
- Musick JA, Harbin MM, Berkeley SA, Burgess GH, Eklund AM, Findley L, Gilmore RG, Golden JT, Ha DS, Huntsman GR, McGovern JC, Parker SJ, Poss SG, Sala E, Schmidt TW, Sedberry GR, Weeks H, Wright SG (2000) Marine, estuarine, and diadromous fish stocks at risk of extinction in North America. *Fisheries* 25:6–30
- NMFS (National Marine Fisheries Service) (1999) Final fishery management plan for Atlantic tunas, swordfish, and sharks. DOC/NMFS/HMS Management Division, Silver Spring, MD.
- NMFS (National Marine Fisheries Service) (2017) Amendment 10 to the 2006 consolidated Atlantic highly migratory species fishery management plan: essential fish habitat and environmental assessment. NOAA/NMFS HMS Management Division, Silver Spring
- O'Toole AC, Murie KJ, Pullen C, Hanson KC, Suski CD, Danylchuk AJ, Cooke SJ (2010) Locomotory activity and depth distribution of adult great barracuda (*Sphyraena barracuda*) in Bahamian coastal habitats determined using acceleration and pressure biotelemetry transmitters. *Mar Freshw Res* 61(12):1446–1456
- Otway NM, Burke AL, Morrison NS, Parker PC (2003) Monitoring and identification of NSW critical habitat sites for conservation of grey nurse sharks. NSW Fish Final Rep Ser 47
- Otway NM, Ellis MT (2011) Pop-up archival satellite tagging of *Carcharias taurus*: movements and depth/temperature-related use of south-eastern Australian waters. *Mar Freshw Res* 62:607–620
- Papastamatiou YP, Watanabe YY, Bradley D, Dee LE, Weng K, Lowe CG, Caselle JE (2015) Drivers of daily routines in an ectothermic marine predator: hunt warm, rest warmer? *PLoS One* 10(6):e0127807
- Payne NL, Gillanders BM, Webber DM, Semmens JM (2010) Interpreting diel activity patterns from acoustic telemetry: the need for controls. *Mar Ecol Prog Ser* 419:295–301
- Payne NL, Smith JA, Meulen DE, Taylor MD, Watanabe YY, Takahashi A et al (2016) Temperature dependence of fish performance in the wild: links with species biogeography and physiological thermal tolerance. *Funct Ecol* 30(6):903–912
- Pedersen MW, Patterson TA, Thygesen UH, Madsen H (2011) Estimating animal behavior and residency from movement data. *Oikos* 120:1281–1290
- Pedersen MW, Weng KC (2013) Estimating individual animal movement from observation networks. *Methods Ecol Evol* 4(10):920–929

- Pincock, DG (2012) False detections: what are they and how to remove them from detection data. Vemco Document #: DOC-004691 Version 03
- Pollard DA, Lincoln Smith MP, Smith AK (1996) The biology and conservation status of the grey nurse shark (*Carcharias taurus* Rafinesque 1810) in New South Wales, Australia. *Aquat Conserv Mar Freshwat Ecosyst* 6(1):1–20
- R Core Team (2016) R: A language and environment for statistical computing. R Foundation for Statistical Computing, Vienna, Austria. URL <https://www.R-project.org/>
- Reebs SG (2002) Plasticity of diel and circadian activity rhythms in fishes. *Rev Fish Biol Fish* 12(4):349–371
- Robbins WD, Peddemors VM, Broadhurst MK, Gray CA (2013) Hooked on fishing? Recreational angling interactions with the critically endangered grey nurse shark *Carcharias taurus* in eastern Australia. *Endanger Species Res* 21(2):161–170
- Schlaff AM, Heupel MR, Simpfendorfer CA (2014) Influence of environmental factors on shark and ray movement, behaviour and habitat use: a review. *Rev Fish Biol Fish* 24:1089–1103
- Schwarz G (1978) Estimating the dimension of a model. *Ann Stat* 6(2):461–464
- Simpfendorfer CA, Yeiser BG, Wiley TR, Poulakis GR, Stevens PW (2011) Environmental influences on the spatial ecology of juvenile smalltooth sawfish (*Pristis pectinata*): results from acoustic monitoring. *PLoS One* 6(2):e16918
- Smale MJ (2005) The diet of the ragged-tooth shark *Carcharias taurus* Rafinesque 1810 in the eastern cape, South Africa. *Afr J Mar Sci* 27(1):331–335
- Smale MJ, Booth AJ, Farquhar MR, Meyer MR, Rochat L (2012) Migration and habitat use of formerly captive and wild raggedtooth sharks (*Carcharias taurus*) on the southeast coast of South Africa. *Mar Biol Res* 8:115–128
- Smith KR, Scarpaci C, Louden BM, Otway NM (2015) Behaviour of aggregated grey nurse sharks *Carcharias taurus* off eastern Australia: similarities and differences among life-history stages and sites. *Endanger Species Res* 27(1):69–85
- Stehfest KM, Lyle JM, Semmens JM (2015) The use of acoustic accelerometer tags to determine seasonal changes in activity and catchability of a recreationally caught marine teleost. *ICES J Mar Sci* 72(8):2512–2520
- Taylor MD, McPhan L, van der Meulen DE, Gray CA, Payne NL (2013) Interactive drivers of activity in a free-ranging estuarine predator. *PLoS One* 8(11):e80962
- Teter SM, Wetherbee BM, Fox DA, Lam CH, Kiefer DA, Shivji M (2015) Migratory patterns and habitat use of the sand tiger shark (*Carcharias taurus*) in the western North Atlantic. *Mar Freshw Res* 66(2):158–169
- Thorson JT, Shelton AO, Ward EJ, Skaug HJ (2015) Geostatistical delta-generalized linear mixed models improve precision for abundance indices for west coast groundfishes. *ICES J Mar Sci* 72:1297–1310
- Thorson JT, Ianelli JN, Kotwicki S (2017) The relative influence of temperature and size-structure on fish distribution shifts: a case-study on walleye Pollock in the Bering Sea. *Fish Fish* 2017:1–12
- Ubeda AJ, Simpfendorfer CA, Heupel MR (2009) Movements of bonnetheads, *Sphyrna tiburo*, as a response to salinity change in a Florida estuary. *Environ Biol Fish* 84:293–303
- Watanuki Y, Niizuma Y, Geir WG, Sato K, Naito Y (2003) Stroke and glide of wing-propelled divers: deep diving seabirds adjust surge frequency to buoyancy change with depth. *Proc R Soc Lond B* 270(1514):483–488
- Watsky M, Gruber SH (1990) Induction and duration of tonic immobility in the lemon shark *Negaprion brevirostris*. *Fish Physiol Biochem* 8:207–210
- Weltz K, Kock AA, Winker H, Attwood C, Sikweyiya M (2013) The influence of environmental variables on the presence of white sharks, *Carcharodon carcharias*, at two popular Cape Town bathing beaches: a generalized additive mixed model. *PLoS ONE* 8(7):e68554
- Whitney NM, Papastamatiou YP, Holland KN, Lowe CG (2007) Use of an acceleration data logger to measure diel activity patterns in captive whitetip reef sharks, *Triaenodon obesus*. *Aquat Living Resour* 20(4):299–305
- Whitney NM, Pratt HL Jr, Pratt TC, Carrier JC (2010) Identifying shark mating behaviour using three-dimensional acceleration loggers. *Endanger Species Res* 10:71–82
- Whitney NM, Papastamatiou YP, Gleiss AC (2012) Integrative multi-sensor tagging: emerging techniques to link elasmobranch behavior, physiology and ecology. In: Carrier JC, Musick JA, Heithaus MR (eds) Biology of sharks and their relatives, 2nd edn. CRC Press, Boca Raton, p 265–290
- Wilson SM, Hinch SG, Eliason EJ, Farrell AP, Cooke SJ (2013) Calibrating acoustic acceleration transmitters for estimating energy use by wild adult Pacific salmon. *Comp Biochem Physiol A Mol Integr Physiol* 164(3):491–498
- Wilson SM, Hinch SG, Drenner SM, Martins EG, Furey NB, Patterson DA, Welch DW, Cooke SJ (2014) Coastal marine and in-river migration behaviour of adult sockeye salmon en route to spawning grounds. *Mar Ecol Prog Ser* 496:71–84
- Winton MV, Fay G, Haas HL, Arendt M, Barco S, James MC, Sasso C, Smolowitz R (2018) Estimating the distribution and relative density of satellite-tagged loggerhead sea turtles using geostatistical mixed effects model. *Mar Ecol Prog Ser* 586:217–232
- Zhu L, Li L, Liang Z (2009) Comparison of six statistical approaches in the selection of appropriate fish growth models. *Chin J Oceanol Limnol* 27:457–467